GPS Constraints on the Kinematics of Continental Deformation

WAYNE THATCHER[1]

U. S. Geological Survey, MS/977, Menlo Park, California 94025

Abstract

Recent GPS observations from the western United States, New Zealand, central Greece, and Japan indicate that present-day continental deformation is typically focused in narrow deforming zones whose extent is much smaller than the intervening largely inactive regions. However, these narrow zones are heterogeneously distributed, reflecting the inherent heterogeneity of continental lithospheric strength and internal buoyancy. Plate driving and resisting forces stress plate boundary zones and plate interiors and drive deformation. These forces change continuously and discontinuously, leading to continental deformation that typically evolves and migrates with time. Magmatic and tectonic processes alter lithospheric rheology and internal buoyancy and also contribute to the time-varying character of continental deformation.

Introduction

THE RELATIVE MOTIONS of oceanic plates and the deformation occurring at their boundaries have long been well understood and are easily quantified. With only rare exceptions, the oceanic plates are not internally deformed. Interplate straining occurs in narrow zones, and this straining is determined by the relative motions of the bounding plates. Magnetic lineations, fracture zone orientations, and earthquake slip vectors record the interplate motion, and these data can be applied to accurately determine the relative rotation rates of the plates. This description has been unanimously accepted for over 30 years and relative rotation (Euler) vectors for the major plates have been regularly updated and refined as new and better data became available (e.g., Minster and Jordan, 1978; Demets et al., 1990).

No comparably simple or agreed upon description yet exists for quantifying active continental deformation. Broad mountain belts, diffuse seismicity, and strong lateral variations in lithospheric structure show that deformation is more complex than in ocean basins. However, the difficulty of obtaining precise estimates of movement rates has long been a major obstacle to quantitative characterization of continental deformation. Seismicity catalogs provide a short and therefore temporally biased record because major faults are often locked (not slipping), and are hence aseismic for the majority of their seismic cycle. Obtaining precise geologic esti-

mates is arduous and labor intensive, and usefully complete coverage exists in only a few limited regions. Until very recently, geodetic estimates of movement rates have been comparably limited. In the absence of firm quantitative constraints two idealized end-member models have been proposed (Figs. 1A and 1B), each with their own strengths and limitations.

At one extreme, deforming zones are comprised of rigid microplates with little internal distortion and with straining localized only at their boundaries (Fig. 1A). Such a description has the advantage of simplicity, with relative motions specified only by Euler vectors. Clear examples of rigid behavior have been demonstrated for several regions, including western Anatolia (McKenzie, 1972), the Tarim Basin (Avouac and Tapponnier, 1993), the Oregon Coast (Wells et al., 1998) and the Sierra Nevada–Great Valley microplate (Argus and Gordon, 1991). However, the finite width of deforming regions is not considered, and many microplates may be needed to characterize the large-scale deformation. Furthermore, buoyancy forces generated by lateral density gradients within the continental lithosphere can produce internal deformation that may not be compatible with the simple Euler vector description.

At the other extreme, deformation is viewed as quasi-continuous, with pervasive internal straining and few, if any, plate-like elements (Fig. 1B). Modeling applications with this point of departure (e.g., England and McKenzie, 1982; Flesch et al., 2000) have the advantage of being physical and process based, so that the kinematics are determined by the prescribed boundary forces, the internal buoyancy

[1]Email: thatcher@usgs.gov

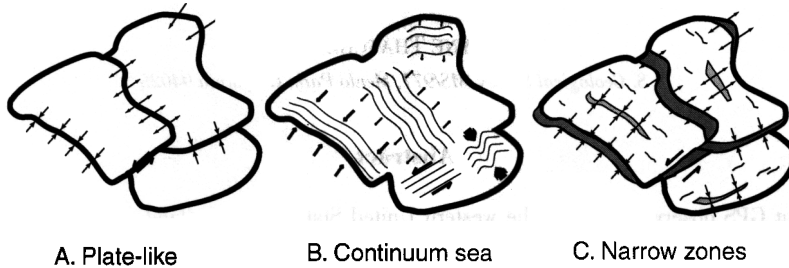A. Plate-like   B. Continuum sea   C. Narrow zones

FIG. 1. Schematic diagrams showing alternative kinematic descriptions of continental deformation. The two end-member models in (A) and (B) have been previously suggested by numerous studies. Results supporting the model sketched in (C) are presented in this paper.

distribution, and the rheology of the lithosphere. However, this approach is necessarily simplified, usually assuming a uniform viscous rheology, and averaging deformation and rheology through the lithospheric column. Thus it is essentially a long-wavelength description that smooths through deforming zones and rigid elements and often ignores lateral variations in rheology.

Which (if either) description of continental deformation is more nearly correct is uncertain. However, the increasing availability of precise space-geodetic estimates of present-day movement rates is rapidly removing the chief obstacle to progress, defining the kinematics of continental deformation over wide regions in many parts of the world. In this paper I review these Global Positioning System (GPS) survey results from a number of active regions worldwide, focusing on their common features and suggesting their implications for the kinematics and dynamics of continental lithosphere deformation.

This review suggests a kinematic model for continental deformation that is shown in Figure 1C. Its most important feature is the concentration of present-day deformation in narrow zones ~10 to ~100 km wide separated by much larger intervening inactive regions. However, the nominally inactive regions are locally interrupted by isolated deforming zones, and rare earthquakes as large as M~7 are more widely distributed. Comparison of the strongly localized patterns of GPS deformation with the broader distribution of Quaternary faults suggests that active deformation may migrate with time.

This paper is organized into seven subsequent sections. First I briefly review well-known features of geodetically measured deformation from California and New Zealand, showing how movements are strongly focused close to the major faults in each region. The main body of the paper consists of case histories that document the observed deformation of four intraplate regions: central Greece, Italy, intraplate Japan, and the western United States. Finally, based on the general features of the deformation, I discuss the role of plate boundary forces, internal buoyancy forces, and rheology in accounting for the observed movement pattern and its temporal evolution. The paper ends with a concluding summary and discussion.

Well-Known Narrow Deforming Zones

In a small number of active regions, ground-based geodetic survey measurements have been made for over a century and have been sufficiently accurate to define the large-scale movement patterns. In California and New Zealand, these results showed that the majority of relative plate motion is accommodated across the major strike-slip fault zones of each region (Savage and Burford, 1973; Thatcher, 1975, 1979a, 1979b; Walcott, 1978). Recent GPS results have brought these features into even sharper focus, as I show here.

Even before the advent of GPS measurements, it was clear that shear straining is concentrated close to the San Andreas fault and its related subparallel strands (e.g., Lisowski et al., 1991). In the San Francisco Bay area (Fig. 2), high fault-parallel velocity gradients are focused in a zone ~100 km wide that spans the San Andreas, Hayward, and Calaveras faults. In addition, GPS measurements have resolved a localized 2–3 mm/yr change in fault-perpendicular velocity associated with thrust faults at the boundary between California's Great Valley and Coast Ranges (Prescott et al., 2001).
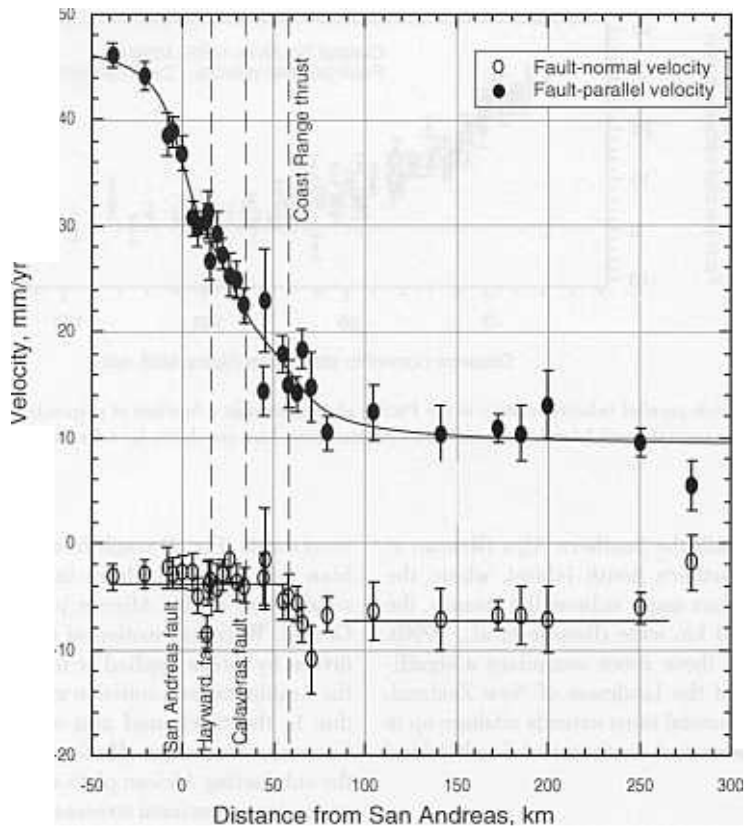
FIG. 2. GPS velocity relative to stable North America plotted as a function of perpendicular distance from the San Andreas fault in the San Francisco Bay area. Both fault-parallel (solid ellipses) and fault-perpendicular (open ellipses) velocity components are plotted along with their one-standard-deviation error bars. The subparallel Hayward and Calaveras faults and the Coast Range thrust are shown for reference. Modified from Prescott et al. (2001).

The smooth distribution of fault-parallel velocity shown in Figure 2 is the result of elastic strain accumulation in the crustal blocks adjacent to each fault. The width of this zone scales with the depth of each of the currently locked (non-slipping) faults of the region, about 10–15 km. The considerable width of this zone, about 120 km, is the result of the superposed effects of straining across the three major strike-slip faults of the San Francisco Bay area. The spacing of these faults (Fig. 2) is comparable to their 10–15 km locking depths. Earthquake fault slip in events of M~7 or greater will eventually release these accumulated strains, generating the block offsets preserved in the geological record across these faults (see Thatcher, 1995, Fig. 4, for details).

Elsewhere in California, geodetic measurements define zones of deformation across the San Andreas system of faults that range from a few km or less to as much as 250 km. On the central creeping segment of the San Andreas, virtually all of the relative motion occurs as aseismic slip, with no strain accumulation in the adjacent crustal blocks (Thatcher, 1979a). In northern California, movements occur over a distance of ~100 km perpendicular to the major faults (Freymueller et al., 1999; Savage et al., 1999), whereas in southern California the zone is 150–250 km wide.

In the South Island of New Zealand, current deformation is also concentrated near the Alpine fault and its major strands. Figure 3 shows that high GPS velocity gradients are located within ~80 km of the fault in central South Island. The pattern of movements is caused by elastic strain accumulation on the Alpine fault and as yet poorly understood
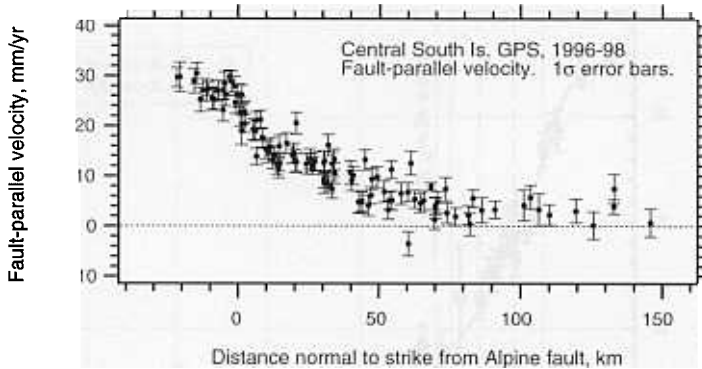
FIG. 3. GPS fault-parallel velocity relative to the Pacific plate plotted as a function of perpendicular distance from the Alpine fault in central South Island. One-standard-deviation error bars are shown for reference (modified from Beavan et al., 1999).

shear zones beneath the Southern Alps (Beavan et al., 1999). In northern South Island, where the Alpine fault has four major subparallel strands, the zone is about 150 km wide (Bourne et al., 1998). Although each of these zones comprises a significant proportion of the landmass of New Zealand, undeformed continental crust extends offshore up to 1000 km northwest and southeast of South Island (Walcott, 1998).

Central Greece

The eastern Mediterranean is a region of diffuse seismicity, widespread active faulting and high rates of present-day crustal deformation. Large-scale

movements (Fig. 4) result from collision of the Arabian and Eurasian plates in eastern Turkey, and subduction of the African plate beneath Aegean Greece. Westward motion of the Anatolian plate is driven by forces applied at its eastern edge due to the Arabia-Eurasia collision and by buoyancy forces due to the thickened and elevated crust of the Caucasus Mountains (McKenzie, 1972). Retreat of the subducting African plate at the Hellenic Trench generates extensional stresses in the backarc region of Greece and western Turkey (Le Pichon, 1982). Collision between Apulia and Albania creates a rigid buttress, funneling the westward motion of Anatolia southwest towards the Hellenic Trench (Jackson, 1994).
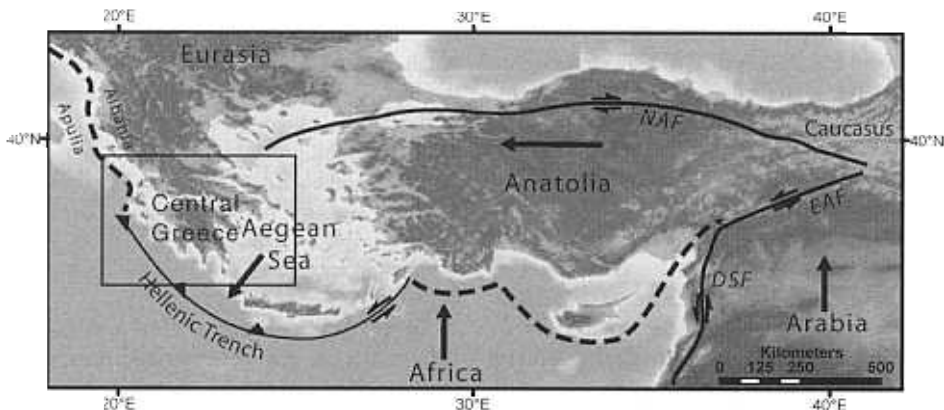

FIG. 4. Large-scale plate tectonic setting of the eastern Mediterranean, showing major plate boundaries and motions of African, Arabian, and Anatolian plates relative to stable Eurasia. Inset box shows area of detail in Figure 5. Abbreviations: NAF = North Anatolian fault; EAF = East Anatolian fault; DSF = Dead Sea fault.
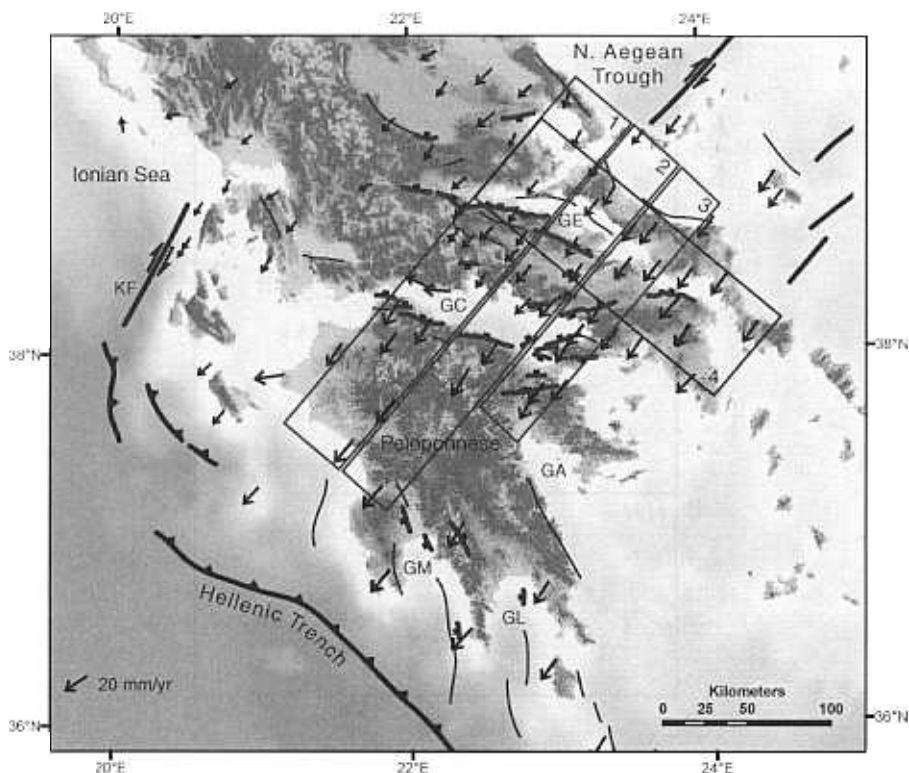
FIG. 5. Regional setting of central Greece. Active faults are shown with sense of strike-slip motion denoted by arrows, solid triangles on overthrust reverse fault blocks, and solid rectangles on subsiding normal fault blocks. GPS vectors are from Clarke et al. (1998) and Cocard et al. (1999). Rectangular boxes show locations of GPS profile data plotted in Figure 6. Abbreviations: GC = Gulf of Corinth; GE = Gulf of Evia; GA = Gulf of Argos; GL = Gulf of Laconia; GM = Gulf of Messenia); KF = Kephalonia fault.

Central Greece lies between the region of strike-slip faulting related to the North Anatolian fault and subduction at the Hellenic Trench (Fig. 5). Clear evidence of strike-slip faulting disappears at the North Aegean Trough, the westernmost extension of the North Anatolian fault. Underthrusting occurs in the Ionian Sea at the Hellenic Trench. In between, extensional stresses due to slab retreat have generated widely distributed normal faulting, spectacular fault morphology, and abundant seismicity. Although these deformation indicators suggest straining is evenly distributed, GPS results are clearly showing that this is not the case.

Figure 5 shows recently determined GPS velocities relative to Eurasia (Clarke et al., 1998; Cocard et al., 1999) superimposed on a fault map of central Greece. Two first-order features are evident. First, the general northwest to southeast increase in veloc-ity is due to the clockwise rotation of north-central Greece relative to Eurasia. This is shown in Profile 4, Figure 6B, where GPS velocities along a NW-SE transect are compared with those expected for the Eurasia/central Greece (EUR/CGR) Euler vector estimated by Le Pichon et al. (1995). Second, there is an abrupt increase in velocity across the Gulf of Corinth. Although evident in the GPS velocity map of Figure 5, its nature is more clearly demonstrated in the velocity profiles plotted in Figure 6A. The high velocity gradient occurs in a zone less than ~30 km wide. Furthermore, extension decreases rapidly from northwest to southeast within a dis-tance of 80 km or less: 18 ± 3 mm/yr in the central Gulf (Profile 1); 10 ± 2 mm/yr in the eastern Gulf (Profile 2); and 3 ± 2 mm/yr farther southeast (Pro-file 3). There is no evidence for significant deforma-tion adjacent to this narrow region. In particular,
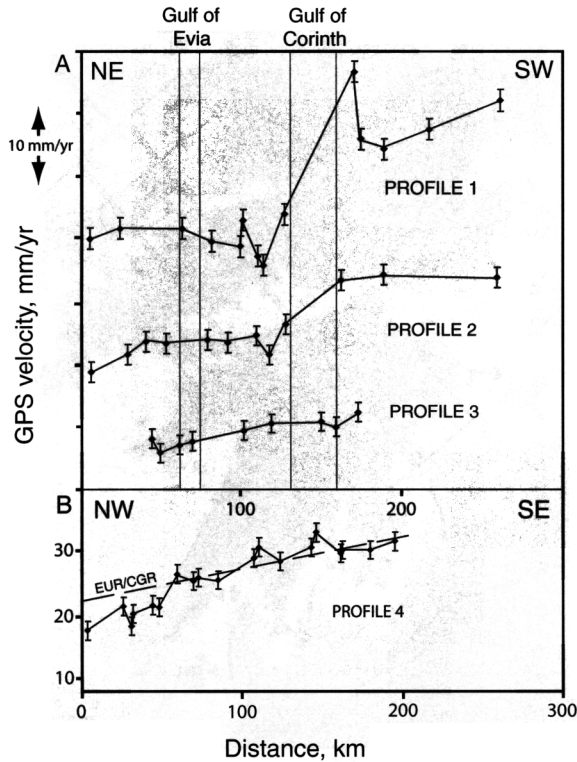
FIG. 6. GPS velocity versus distance along profiles indicated by boxed regions in Figure 5. A. NE-SW profiles. GPS velocity profiles are offset for clarity. Locations of Gulf of Corinth and Gulf of Evia are shown for reference. B. NW-SE profile north of Gulf of Corinth, with velocities relative to fixed Eurasia. Dashed line shows predicted velocities for rotation of north-central Greece relative to Eurasia about a Euler pole located near 41°N and 18°E, with a rotation rate of 2.8°/m.y. (Le Pichon et al., 1995)

there is no detectable relative motion across the Gulf of Evia, where late Quaternary fault scarps have been identified and an M = 6.9 earthquake occurred in 1894 (Richter, 1958, pp. 617–618).

Elsewhere in central Greece, significant straining is either absent or poorly defined. West of the Gulf of Corinth, the few available GPS vectors suggest extension of as much as ~10 mm/yr but do not otherwise constrain it. GPS results of Cocard et al. (1999) indicate significant shear straining is localized across the Kephalonia fault (KF, Fig. 5). Analysis of triangulation data and its incorporation with early GPS and Satellite Laser Ranging (SLR) results suggested as much as 3–10 mm/yr of extension across the normal fault–bounded Gulfs of Argos, Laconia, and Messina of the eastern and southern Peloponnese (GA, GL, GM, Fig. 5) (Le Pichon et al., 1995). However, the newer GPS results shown in Figure 5 indicate that any

extension in these regions must be occurring at significantly lower rates.

Based on the GPS results, Figure 7 shows a speculative mapping of the present-day zones of deformation in central Greece. Strike-slip faulting is localized on the North Aegean Trough and possibly several subparallel faults to the south. Convergence and thrust faulting occurs in northwestern Greece and along the Hellenic Trench, with the two zones offset by strike-slip motion across the Kephalonia fault. Significant extensional deformation is confined to the Gulf of Corinth, with possible continuation to the west, and perhaps in other localized zones in the Gulf of Evia and southern Peloponnese. The pattern shown in Figure 7 has several similarities with that described by Le Pichon et al. (1995), who first suggested extension in central Greece was largely localized in the Gulf of Corinth due to counterclockwise rotation of the Anatolian plate (and the
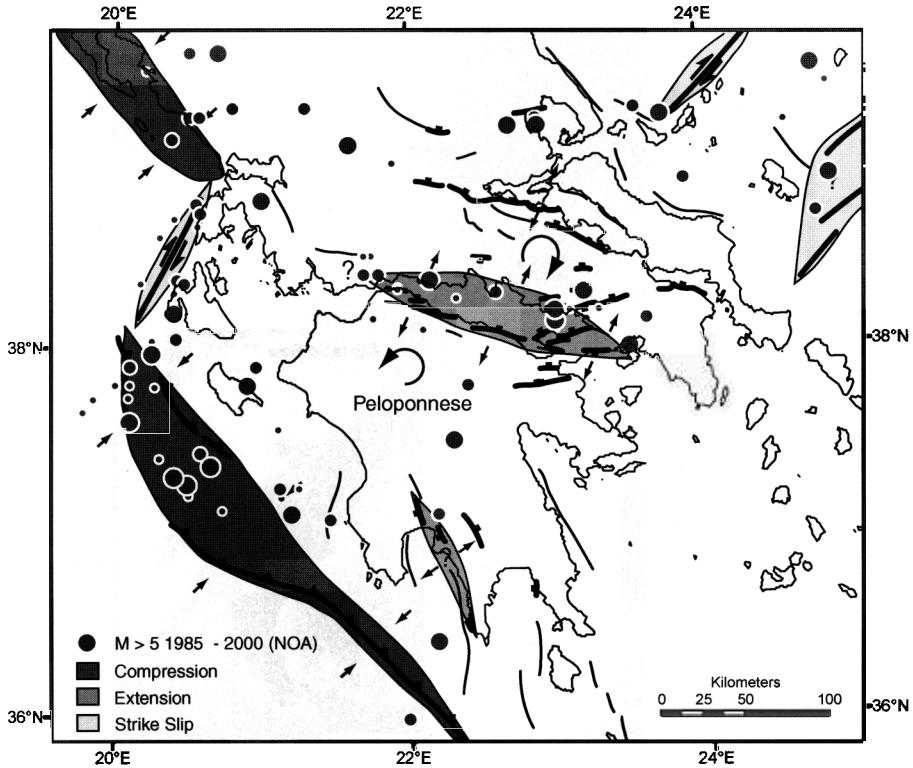
FIG. 7. Schematic mapping of zones of localized deformation in central Greece suggested from recent GPS survey results. Active faults are depicted in the same way as in Figure 5. Earthquakes with M>5 during 1985–2000 are from the National Observatory of Athens.

Peloponnese) and clockwise rotation of north-central Greece. However, the rates of extension west of the Gulf of Corinth are uncertain and may not be explained by strictly rigid motions of the bounding blocks. If the deformation is indeed confined laterally as shown in Figure 7, the GPS data do not define how this localized extension is accommodated within the adjacent crustal blocks.

Figure 7 also shows that recent M>5 earthquakes and many active faults are located within or close to the proposed deformation zones. Nonetheless, both significant earthquakes and identified young faults lie outside the deforming regions defined largely from GPS measurements.

Italian Peninsula

The Apennine Mountains form the rugged topographic crest of the Italian Peninsula and have been the site of localized normal faulting during the past 1–2 m.y. Prior to this time, this same region was under compression, which has apparently migrated eastward with time (Cavinato and Decelles, 1999). Detailed seismotectonic investigations carried out over the past decade have defined the main sources of active faulting in the Peninsula (Valensise and Pantosti, 2001). Remarkably, they show that normal faults are preferentially located in a narrow zone near the Apennine crest (Fig. 8). A recently active fold-thrust belt is located farther to the east, defined by structures in the Po Valley of northern Italy (PV, Fig. 8), reverse faults near the Adriatic coast of central and northern Italy, and scattered thrust focal mechanisms in the same region. Figure 8 shows that earthquakes of M = 5 or greater are also preferentially located close to the identified seismogenic source zones. GPS results are not yet available with sufficient density to define the detailed distribution of present-day deformation. However, within a few years, campaign GPS networks currently being established will determine the pattern of straining across both the localized normal fault zones and
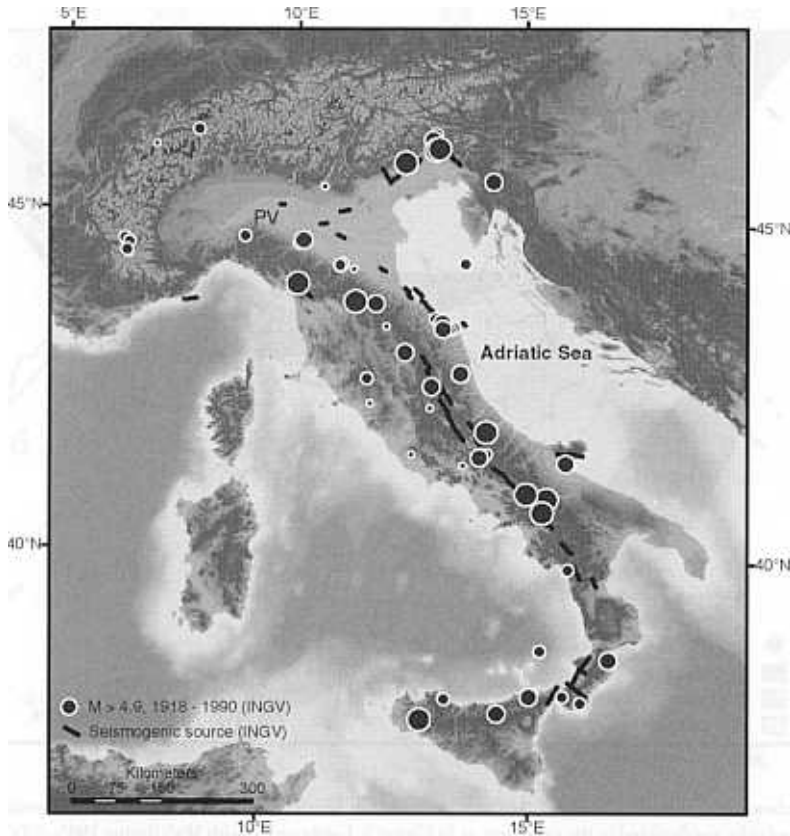
FIG. 8. Topography of the Italian Peninsula, with seismic source zones and earthquakes from data base of Valensise and Pantosti (2001). Abbreviations: PV = Po Valley.

regions of apparently contemporaneous thrusting that lie to the east of the Apennines.

Intraplate Japan

The Japanese Islands are among the most intensely deforming regions on Earth. The best-known effects are due to the frequent large and great underthrust earthquakes that occur near the Pacific, Philippine Sea, and Japan Sea coasts of Japan. Perhaps less appreciated is the significant and well-documented intraplate deformation that occurs onshore. Japan is surrounded by plates that converge upon it (Fig. 9). The intraplate stress field is therefore dominantly compressive, manifesting itself in a complex pattern of reverse and strike-slip faults. The rather even distribution of faults might suggest broadly distributed deformation, but recent GPS results again indicate otherwise.

The broad outlines of the current movement pattern have been revealed from the century-long record of triangulation and leveling surveys. However, GPS measurements made during the past five years have brought this pattern into much sharper focus. A network of nearly 1000 continuously recording GPS sites was installed beginning in 1993. Results from this network have revealed the character of inter-plate strain accumulation related to subduction of the Pacific and Philippine Sea plates (Le Pichon et al., 1998; Mazzotti et al., 2000; Sagiya, 1999; Sagiya et al., 2000; Nishimura et al., 2001b). Although the stations are less densely distributed away from these subduction zones, they are sufficient to determine the smaller intraplate strain rate distribution over most of Japan (Sagiya et al., 2000; Mazzotti et al., 2001).

Because the intraplate region is dominantly under compression, a mapping of the dilational
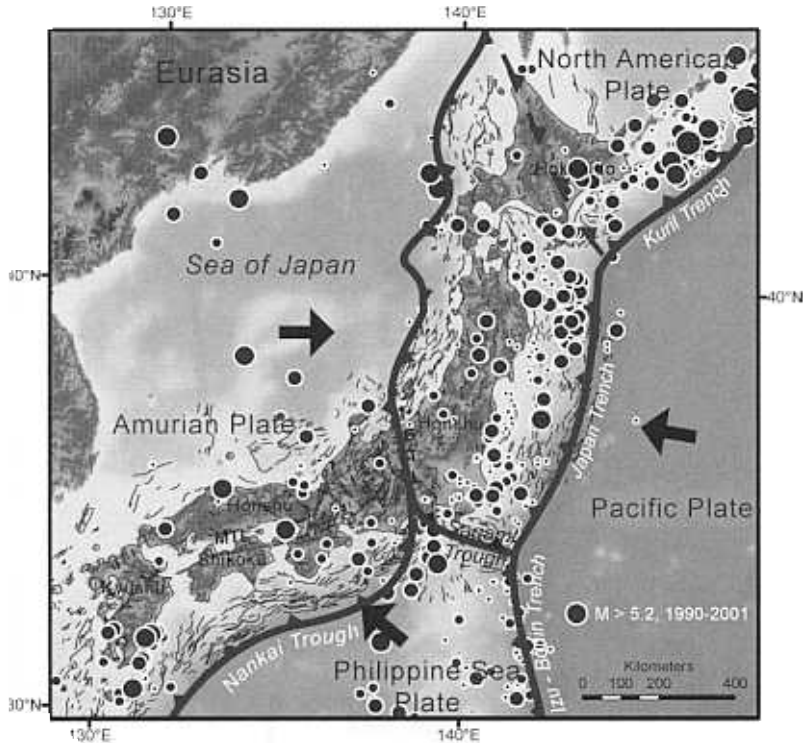
FIG. 9. Plate tectonic setting of the Japanese Islands, showing major boundaries and motions relative to Japan. Faults are from the Research Group for Active Faults of Japan (1991). Abbreviations: MTL = Median Tectonic Line; ISTL = Itoigawa-Shizuoka Tectonic Line.

strain rate field (Fig. 10) is representative of the present-day distribution of GPS deformation. The strain rate field shown in Figure 10 includes effects of both intraplate deformation and elastic straining related to subduction near the Pacific and Philippine Sea coasts. Nonetheless, the effects are spatially distinct and easily distinguished. For example, compression in south-central Honshu and Shikoku is due to interseismic strain buildup on the Sagami Trough, site of the great 1923 Kanto earthquake (Wald and Sommerville, 1995). Similarly, compression near the coast of southwestern Honshu is due to cyclic deformation related to great Nankai Trough earthquakes like those in 1944 and 1946 (Sagiya and Thatcher, 1999). Tensile straining near the coast of southwestern Hokkaido is likely an after-effect of the M = 7.7 Hokkaido Nansen-oki earthquake (Tanioka et al., 1995) on the adjacent subduction boundary. Finally, high rates of tensile strain offshore from central Honshu are due to magmatic activity during 1998–2000 (Nishimura et al., 2001a).

The remaining features shown in Figure 10 seem to reflect steady-state intraplate deformation that is concentrated in a small number of distinct regions. Compression occurs in a narrow zone at least 400 km long bordering the Japan Sea coast of central Honshu. Sagiya et al. (2000) called this the Niigata-Kyoto Tectonic Zone, and suggested that it may extend an additional ~300 km southwest. Smaller regions of compression are located in north-central Honshu, and northeast Hokkaido. Extension in central and western Kyushu is related to volcanic activity and backarc spreading that also occurs in the Okinawa Trough to the southwest.

Recent densification of the Japanese continuous GPS net has identified localized deformation that was not previously resolved. Sagiya et al. (2002) located a zone of high GPS velocity gradient ~15 km wide across the Itoigawa-Shizuoka Tectonic Line (ISTL, Fig. 9) in central Honshu. Tabei et al. (2002) used a mix of campaign and new continuous GPS sites with ~5–10 km spacing to detect localized
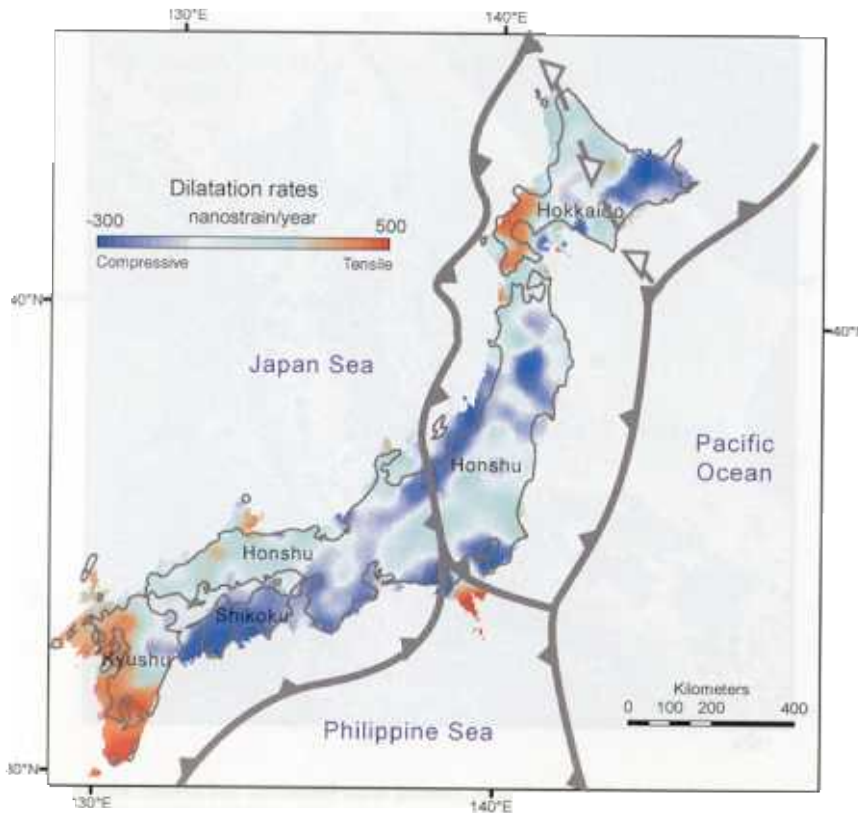
FIG. 10. Dilatation strain rate determined from GPS measurements (modified from Sagiya et al., 2000). Inferred major plate boundaries are shown for reference.

straining across the Median Tectonic Line (MTL, Fig. 9) in Shikoku.

Western United States

The western United States (Fig. 11) is a region of high seismicity, widely distributed active faulting, and increasingly well documented crustal deformation. Interactions with the bounding oceanic plates of the Northeast Pacific concentrate most of the interplate strain near the continent-ocean boundary, but significant deformation occurs more than 1000 km inland.

GPS results

In California, 70–80 % of the 51–53 mm/yr Pacific-North America relative motion (Demets and Dixon, 1999) is taken up by strike-slip faulting along the San Andreas fault system (Thatcher,

1990). As shown in Figure 2 and discussed in the section on well-known deforming zones, the San Andreas straining is localized in a zone of varying width along strike, ranging from less than a km in central California to ~100–250 km to the north and south. East of the San Andreas, the rigid Sierra Nevada microplate is being translated ~N 40° W at 12–14 mm/yr with respect to stable North America (Argus and Gordon, 1991; Dixon et al., 2000).

Oblique convergence between the Juan de Fuca plate and the Pacific Northwest produces subduction beneath northern California, Oregon, and Washington and northward motion of a forearc block farther landward. GPS velocities from networks near the coast are matched by models of elastic strain accumulation due to deep aseismic slip occurring at 30–40 mm/yr (Savage et al., 2000; McCaffrey et al., 2000). However, residual motions there and farther
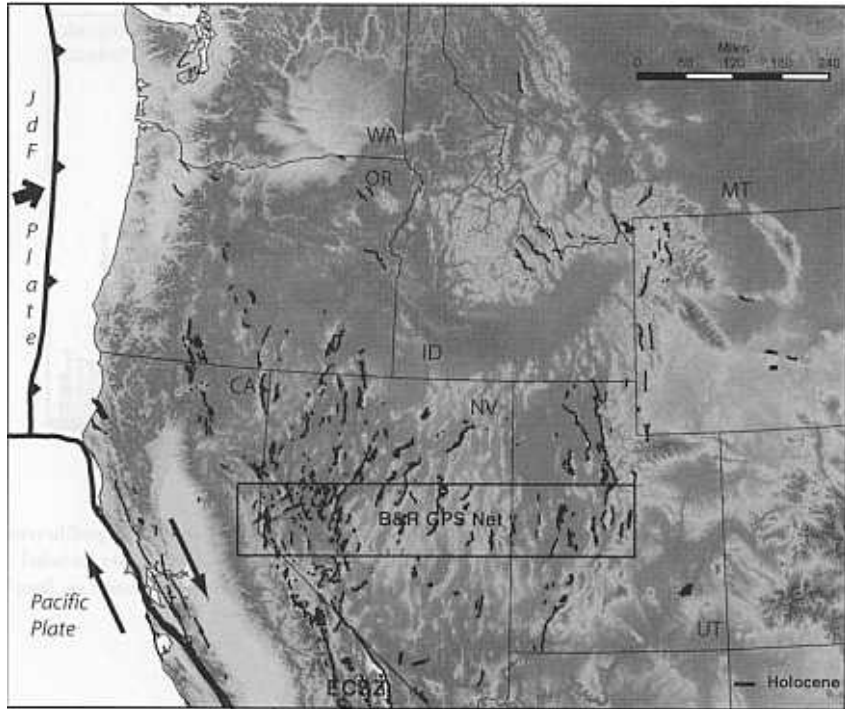
FIG. 11. Topography, Holocene faults, and plate tectonic setting of western United States. Abbreviations: JdF = Juan de Fuca plate; ECSZ = Eastern California shear zone. The rectangular box (lower center) encloses central Basin and range (B&R) GPS network for which the velocity profile is plotted in Figure 12. States are abbreviated as follows: CA = California; ID = Idaho; MT = Montana; NV = Nevada; OR = Oregon; WA = Washington; UT = Utah.

inland cannot be explained in this way. These data require clockwise rotation relative to stable North America of a crustal block, the Oregon Coast microplate, which lies between the subduction zone and the Cascade volcanic arc (Wells et al., 1998; Svarc et al., 2002).

East of the Sierra Nevada and Oregon Coast microplates, Holocene faulting, seismicity, and fault-related topographic features extend farther eastward 100–1000 km (Fig. 11). Relative motions of as much as 12–14 mm/yr are distributed across this region, and although the detailed pattern is well mapped by GPS in only a few regions, recent results have revealed several characteristic features. Immediately east of the Sierra Nevada, relative right-lateral motion of 12 mm/yr is accommodated within a region ~100 km wide (Gan et al., 2000), the Eastern California shear zone (ECSZ, see Fig. 11), that encompasses the major Holocene faults at this latitude. About 300 km farther north, across the central Basin

and Range, faulting is spread over more than 800 km E-W. However, as Figure 12 shows, GPS-measured deformation is not distributed evenly. Instead, straining is concentrated near the eastern and western boundaries of the Basin and Range Province. Adjacent to the Colorado Plateau, 3 ± 1 mm/yr of extension occurs across the Wasatch fault zone. Very little, if any, straining occurs in the central and eastern Basin and Range between latitudes 112° and 118° W. The remainder of the ~12 mm/yr of relative motion between the Colorado Plateau (essentially stable North America) and the Sierra Nevada microplate occurs between 118° and 120° W. It is accommodated across the Central Nevada seismic zone (4 ± 1 mm/yr) and the Northern Walker Lane fault zone (6 ± 2 mm/yr). Recent campaign GPS results from central and western Nevada (Svarc et al., 2002) have confirmed this essential picture. A complementary ~800 km aperture continuous GPS network lying to the north of the one shown in Figure 12 indicates
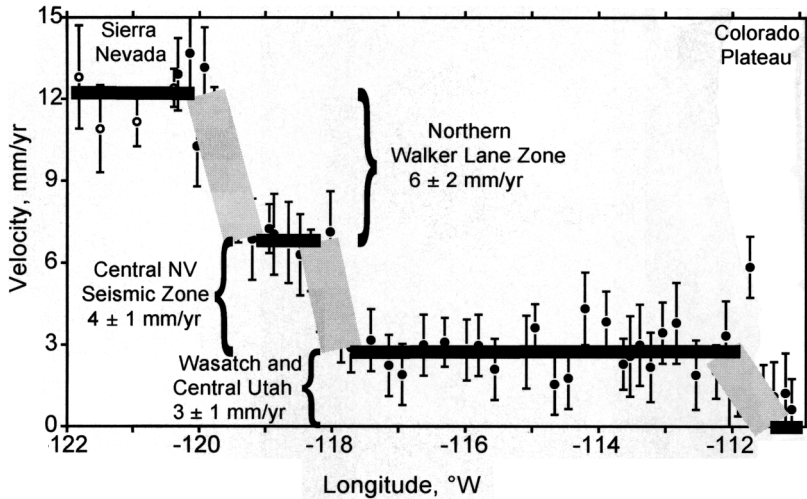
FIG. 12. Magnitude of GPS velocity with respect to stable North America plotted on west to east profile versus longitude from Sierra Nevada microplate to Colorado Plateau. Solid lines show average of velocities over included longitude range. Grey bars are interpreted high-velocity gradients, with velocity increment as indicated. Results are from Thatcher et al. (1999).

very similar results (Bennett et al., 1998). However, these more precise but less densely distributed data suggest that low but resolvable E-W extension may be occurring between 112° and 118° in this region.

Seismicity and Holocene faulting

Over vast areas of the rest of the interior western United States, GPS results are not yet available to supply quantitative constraints on the kinematics of deformation. However, the distribution of seismic activity and Holocene faults (Fig. 13) provides suggestive clues that may be useful. First, seismicity bounds both the western and eastern margins of the Sierra Nevada microplate, generally mimicking the distribution of GPS straining where it has been determined. Several additional quasi-continuous bands of earthquake epicenters are evident in Figure 13. One extends west to east across southern Nevada. A diffuse zone, called the Intermountain seismic belt (Smith and Arabaez, 1991) extends from southwestern Utah, over 800 km NNE to Yellowstone Caldera (YS) in NW Wyoming. Clusters of epicenters extend west from Yellowstone for ~400 km to west-central Idaho, and northwest from Yellowstone through western Montana. Although diffuse activity extends over a much larger area, there is a general tendency for seismicity to be concentrated where the density of Holocene faults is highest.

Distribution of present-day deformation

Figure 14 shows a speculative mapping of the major deformation zones of the western United States based largely on the currently available GPS results supplemented by active fault and seismicity distributions. Compression and underthrusting at the Cascadia subduction zone accommodates virtually all of the convergence between the Juan de Fuca and North American plates. Strike-slip deformation occurs adjacent to the Sierra Nevada microplate in zones much smaller than the dimensions of the microplate itself. Northwestward translation of the Sierra Nevada at ~12 mm/yr creates a zone of north-south compression in northern California and southern Oregon, but the extent of this region and the convergence rate across it are not yet determined. Clockwise rotation of the Oregon Coast microplate relative to stable North America translates this microplate toward the rigid buttress of northern Washington and southwestern Canada, generating N-S compression in western Washington (Wells et al., 1998). Again, the rate of convergence and the width of the deformation zone are not yet well constrained (but see Khazaradze et al., 1999). Throughout the rest of the interior of the western United States, extension dominates, and where it has been well determined, the straining is channeled into narrow deforming zones. Not enough GPS
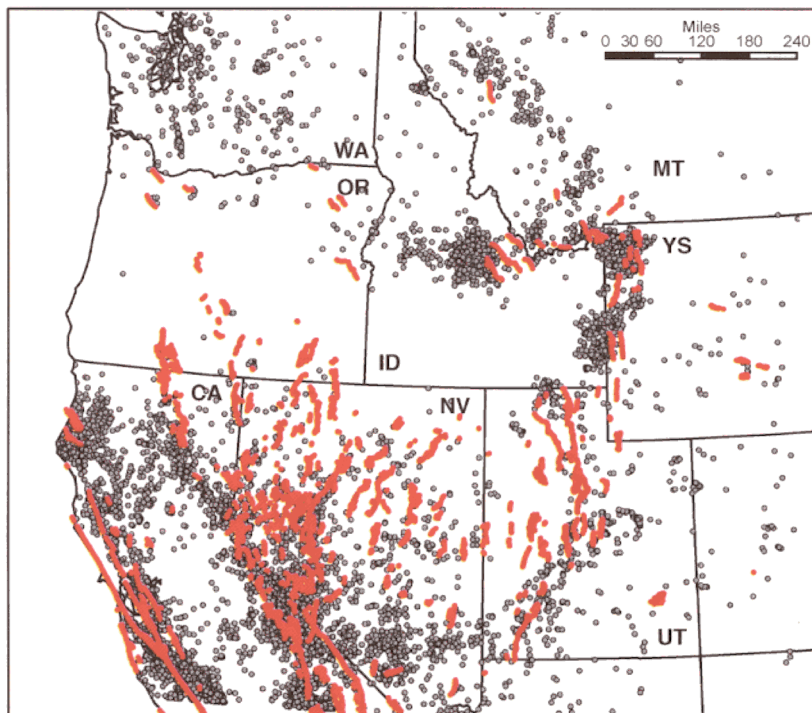
FIG. 13. Western U.S. seismicity and Holocene faults. Abbreviations: YS = Yellowstone caldera. State abbreviati
are the same as those used in Figure 11.

data are yet available to be sure of the along-strike extent of these deforming zones, but the distribution of seismicity and faulting suggests they may be isolated and laterally discontinuous.

Distribution of Quaternary faulting

Although I have thus far limited attention to Holocene faults, it is important to note that the distribution of faults that have demonstrated slip older than Holocene is much more extensive. Indeed as Figure 15 shows, at successively longer time intervals, the distribution becomes more and more widespread. For example, including all faults with proven slip since early Quaternary (up to 1.8 Ma BP) reveals an almost continuous mesh of faults from the California-Nevada border to central Utah (Fig. 15D).

There are at least two reasons for this. First, faults with very low slip rates are displaced infrequently and may not have slipped in the Holocene (past 10 ka) or even the late Quaternary (past 125 ka). However, it is also very likely that many of the older faults are now inactive. In either case, the fault distributions shown in Figures 15B, 15C, and 15D

alone will not be reliable guides to quantitative mapping of current deformation. In many regions of the world less well mapped than the western U. S., faults designated as "active" include those much older than Holocene. In these cases Figure 15 suggests such maps may be misleading representations of the distribution of current activity.

Geoid height and gravitational potential energy

Variations in the geoid height, the reference equipotential surface derived from Earth's gravity field, reflect lateral density gradients in the Earth that are supported by internal stresses. For length scales longer than the lithospheric thickness and assuming local isostatic compensation, gradients in geoid height are linearly related to gradients in gravitational potential energy (GPE) (Coblenz et al., 1994). GPE gradients in turn can be related to stress gradients averaged over the thickness of the lithosphere (England and McKenzie, 1982). Geoid variations can thus be used to assess the distribution of buoyancy forces available to drive lithospheric deformation.
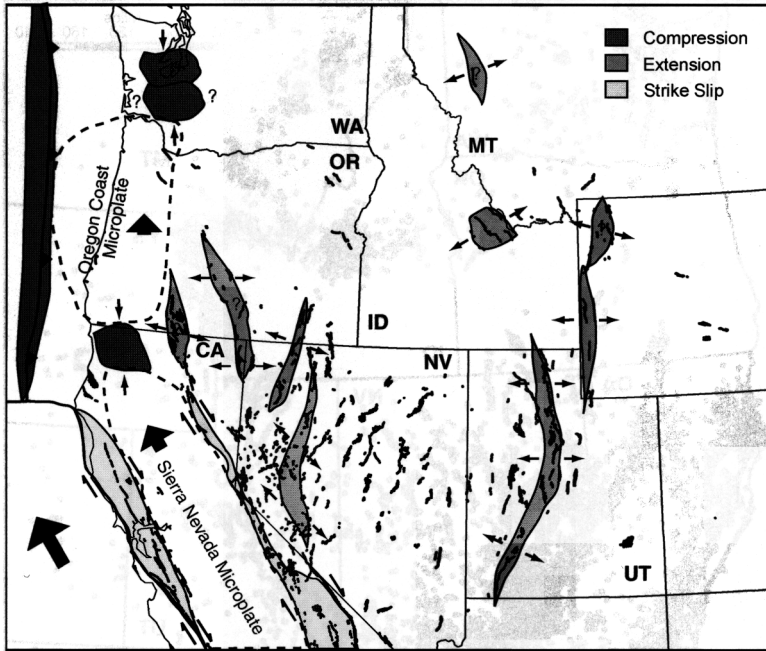
FIG. 14. Schematic mapping of zones of localized deformation in the western United States suggested from recent GPS survey results, Holocene faults, and seismicity.

The distribution of geoid height within the western United States is superimposed on the Holocene fault map in Figure 16 (Hammond and Thatcher, 2001). Strong lateral gradients extend approximately radially from the Yellowstone region, reflecting both lithospheric stress gradients and dynamical support from upper mantle buoyancy. Active normal faults south and west of Yellowstone appear to owe their origin to these strong GPE gradients. Similarly, the strong geoid gradient in eastern California generates extensional stresses at the eastern boundary of the Sierra Nevada microplate, and accounts for the normal faulting occurring there. More subtle gradients in central Utah are consistent with extension across the Wasatch fault zone. Significant geoid gradients also occur in regions like the central Rocky Mountains, where faulting is absent. As is discussed below, stress gradients in such regions can be supported by stronger lithosphere without significant deformation.

Dynamics of Deformation

The patterns and rates of continental deformation are determined by both the forces applied to the lithosphere and by its rheology. This is shown schematically in Figure 17 for the North American plate. Forces applied at its boundaries include those due to: (1) the elevation of the mid-ocean ridges ("ridge-push" force F_{RP}); (2) resistance along transform faults (F_{TR}); (3) pull of the lithosphere toward subduction zones (F_{TS}, the "trench-suction" force); and (4) driving or resisting forces applied at the base of the lithosphere (F_{CD}) (Forsyth and Uyeda, 1975). Lateral density gradients are widely distributed within the continental lithosphere and generate internal driving forces (GPE, Fig. 17A). Rheological laws specify the deformation response of the lithosphere to applied forces. These forces, transmitted by the lithospheric stress guide (the strong upper parts of the plates) determine the intraplate stress field available to drive deformation (Zoback et al., 1989). The spatial distribution of rheology (Fig. 17B), along with the applied forces, then determines the deformation field (Fig. 17C).

Both internal forces and rheology are expected to be very heterogeneous in continental lithosphere. The density distribution is a consequence of the long and complex history of continental lithosphere,
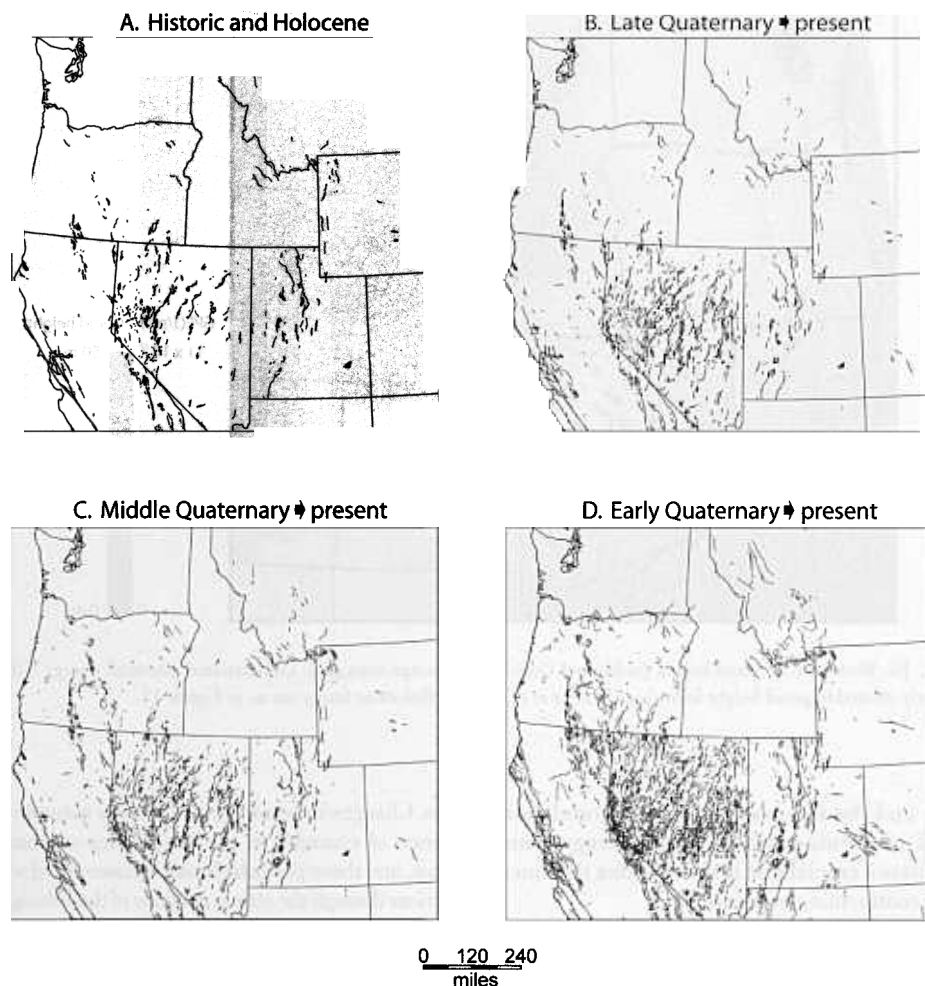
FIG. 15. Western U.S. faults. A. Historic and Holocene. B. Late Quaternary to present. C. Middle Quaternary t present. D. Early Quaternary to present. Faults are from unpublished data of M. Machette and R. Dart (pers. commun. 2002). Fault data from Washington state are not yet available.

and includes effects of magmatism, tectonism, and accretion (e.g., see Mooney et al., 2002). Major fault zones like the San Andreas support much lower shear stress than the surrounding crustal blocks (Mount and Suppe, 1987; Zoback et al., 1987), creating important strength heterogeneities. The rheology of the ductile lithosphere is strongly dependent upon both temperature and composition (Kohlstedt et al., 1995). Modest variations in composition and geothermal gradient thus lead to lateral gradients in lithospheric viscosity of several orders of magnitude (e.g., Sonder and England, 1986).

GPS observations reported here indicate strong strain localization in continental lithosphere both at major plate boundaries and in intraplate regions. Following the logic of Figure 17, this localization could be due to either heterogeneity in local forces or in local strength. Forces due to plate interactions in some cases are largest near the major plate boundaries, where most but not all of the observed deformation is concentrated. Internal buoyancy forces available to cause deformation will be largest near lithospheric density contrasts. However, the very local nature of the observed GPS velocity
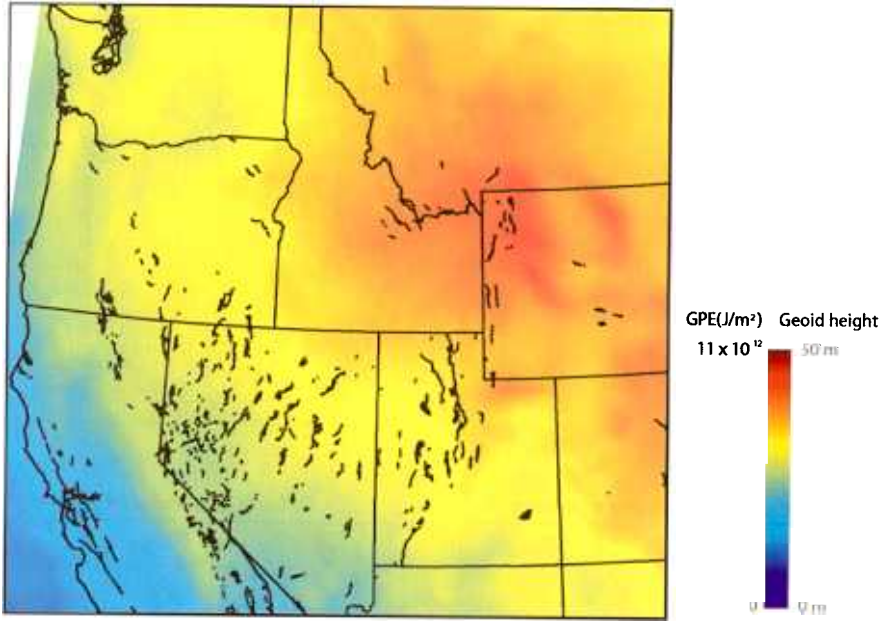
FIG. 16. Western U.S. geoid height (unfiltered Geoid 99, www.ngs.noaa.gov). Gravitational potential energy (GPE) is linearly related to geoid height following Coblenz et al. (1994). Holocene faults are as in Figure 11.

gradients and the frequent absence of correlation with GPE gradients suggests that heterogeneous strength plays a crucial role in determining the kinematics of continental deformation.

Forces available to cause deformation vary naturally with time in both continuous and discontinuous ways. Changes in boundary forces are a natural consequence of changes in the kinematics of bounding plates, and these perturbations are transmitted to plate interiors through the strong portions of the lithosphere.

Abrupt changes in bounding oceanic plate motions have had well-documented effects on style
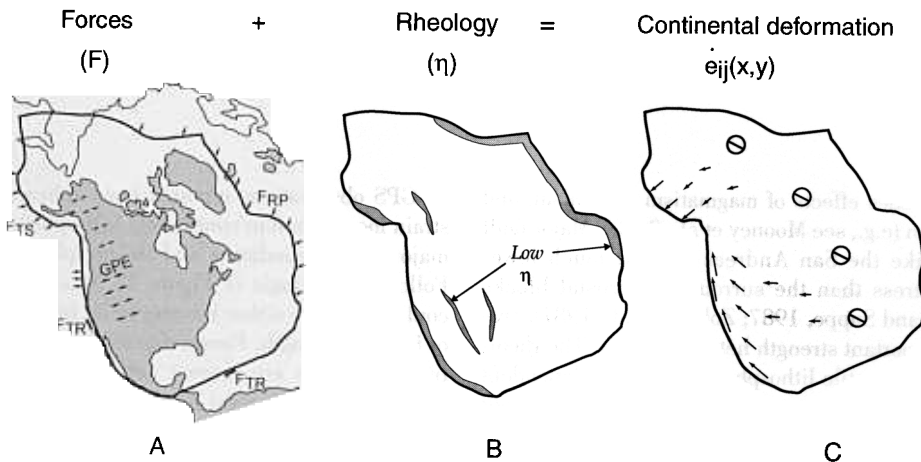

FIG. 17. Schematic diagram illustrating how applied boundary and internal forces and lithospheric rheology determine how continents deform.
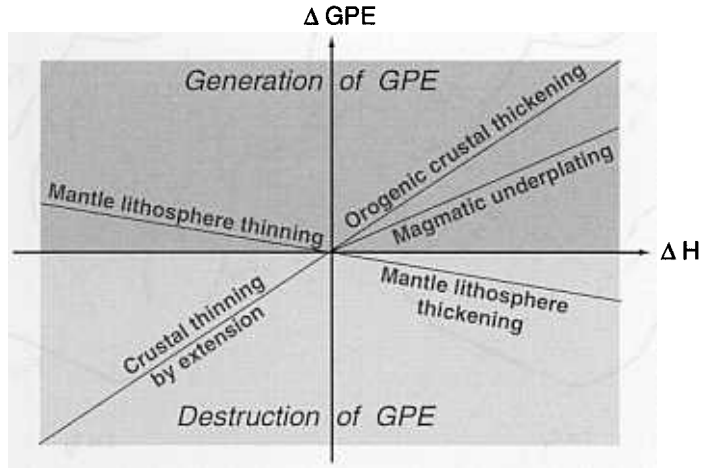
FIG. 18. Schematic plot showing effects of changes in thickness of crust and mantle lithosphere (ΔH) on changes in gravitational potential energy (ΔGPE).

and rates of deformation of adjacent continental plate interiors. For example a ~20° change in the orientation of the Pacific–North American plate motion vector at ~8 Ma (Atwater and Stock, 1998) was approximately coincident with a change from ~E-W extension to NNW-SSE oblique extension in the western U. S. Basin and Range province (Zoback et al., 1983; Wernicke and Snow, 1998). A similar change in Pacific-Australian plate motion at ~6.4 Ma accompanied a change from predominantly strike-slip to oblique compression in the New Zealand plate boundary zone (Walcott, 1998). The relative motion between the Indian and African plates changed at ~8 Ma (Demets et al., 2002). This could have been a cause or an effect of a pulse of uplift of the Tibetan Plateau, which may have led to break-up of the Indo-Australian plate and compression and plate buckling along the Ninety East Ridge (Royer and Gordon, 1997).

Changes in the geometric configurations of adjacent plates can also be gradual and incremental. For example, except for the ridge-ridge-ridge case, triple junctions are intrinsically unstable (McKenzie and Morgan, 1969) and will evolve with time. Off northern California, the Mendocino triple junction migrates northward at ~50 km/Ma, increasing the length of the San Andreas transform at the expense of the Cascadia subduction zone. This migration then has the effect of increasing net F_{TR} and decreasing net F_{TS} along the plate boundary zone. Late Cenozoic changes in the shape and length of

the Hellenic Trench due to slab rollback (Le Pichon, 1982) will lead to temporal change in the intraplate backarc stress field, and the patterns and rates of continental extension in central Greece.

Active tectonic and magmatic processes alter both applied forces and rheology, which also encourage the temporal migration of patterns of deformation. This is shown schematically in Figure 18, which illustrates how changes in crust and mantle lithospheric thickness (ΔH) change the gravitational potential energy (ΔGPE) of a column of lithosphere. Details depend on the density distribution, and the relations between ΔH and ΔGPE in general are not linear (see Lachenbruch and Morgan, 1990; Jones et al., 1996). However, the general behavior is similar to that shown in Figure 18. Thickening of the crust, either by tectonic shortening or magmatic underplating, increases GPE and extensional thinning decreases it. If the mantle lithosphere is denser than the underlying asthenosphere, thickening by conductive cooling decreases GPE, and thinning by delamination increases GPE.

GPE may be liberated by deformation following processes such as magmatism that weaken the lithosphere. For example, migration of the Yellowstone hotspot during the past 16 m.y. would have continually changed both the GPE distribution and the lithospheric strength along the hotspot track, leading to localized deformation in its vicinity. On the other hand, GPE changes may be insufficient to cause deformation, and these internal force changes
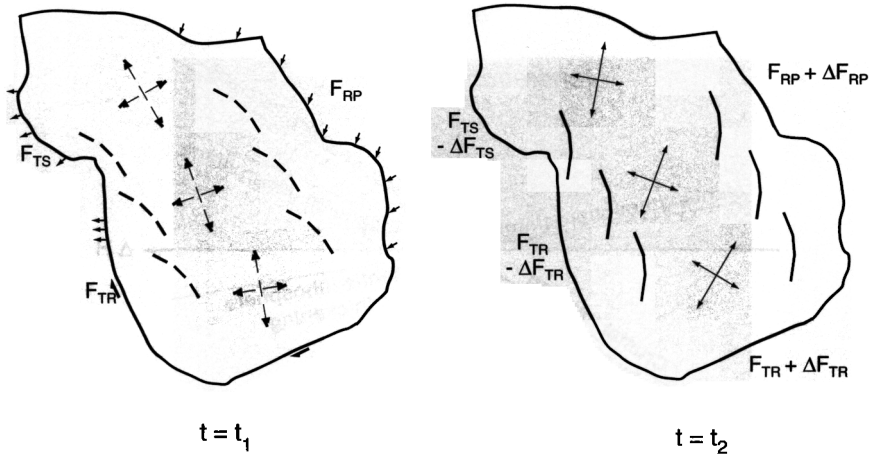
FIG. 19. Effect of changing plate boundary forces on intraplate stress field and fault patterns.

would be supported by the local strength of the lithosphere.

The tectonic effect of changing boundary and internal forces depends both on the pre-existing stress field and the rheology or strength distribution within the continental lithosphere. The magnitude and orientation of intraplate stress changes caused by each driving force increment can be determined for a specified plate rheology, for example uniformly viscous (e.g., England et al., 1985) or perfectly elastic (e.g., Richardson and Reding, 1991). However, the intrinsic material rheology is likely to be spatially quite heterogeneous and not well constrained (Fig. 17B); some faults support lower stresses than others (Mount and Suppe, 1987; Zoback et al., 1987), so determining stress field changes precisely is not yet possible.

Nonetheless, the tectonic effects are conceptually straightforward to understand (Fig. 19). Each force increment changes the intraplate stress field (dashed to solid horizontal principal stress axes, Fig. 19), altering the shearing and normal stresses across active faults and inactive potential failure planes. The magnitude of the effect depends upon the force increment and the pre-existing stress field, either encouraging or discouraging fault slip. Some faults may be unaffected because stress changes are too small. Other faults, especially weak ones, may speed up or slow down due to incremental stress changes. However, under the new stress regime, some subset of faults may become less favorably oriented and become frictionally locked (Sibson, 1985)

(dashed faults, Fig. 19). Still others may be reactivated or new, optimally oriented faults may be created (solid faults, Fig. 19) (Sibson, 1985). Reactivation may be preferentially localized in regions with locally higher ambient stress. For example, these include areas where higher GPE is stored in the lithosphere due to previous tectonism (e.g., thickened crust in inactiveorogenic belts). If, as suggested by Zoback and Townend (2001), the crust is almost everywhere critically stressed (i.e., very near a state of frictional fault failure), then small stress increments could significantly alter pre-existing deformation patterns.

Discussion and Summary

It is commonly accepted that continental deformation is distributed widely, and some indicators of deformation (seismicity, late Cenozoic faulting, regional topographic relief) suggest broad deformation zones. However, qualitative indications of active deformation can be misleading. In many active regions, erosion and tectonism are in balance, and very low rates of slip on inclined faults can generate significant steady-state topography. However, in currently inactive regions, erosion rates are very low, much less than rates of vertical movement in even moderately active deforming zones. For example, Matmon et al. (2003) showed that both current and Cenozoic erosion rates in the central Appalachians are 25–35 m/Ma. Therefore landscape relief provides evidence for current activity, but preserves

it over long periods, millions to tens of millions of years. Secondly, background seismicity is a qualitative measure of tectonic activity, and only the largest earthquakes contribute significantly to representative long-term deformation rates, so the spatial distribution of all smaller events can be misleading. Finally, many mappings of "active" faults encompass features up to several Ma old that are not necessarily representative of current activity.

In contrast, space geodetic observations of movement rates provide quantitative measures that may be more reliable guides to present-day activity. This evidence is just now emerging in many regions of the world. A review of GPS observations from the western United States, New Zealand, central Greece, and Japan suggests that present-day continental deformation is confined to narrow zones ~10–100 km wide. This localization occurs both at major plate boundaries and within adjoining intraplate regions. Because of their modest widths, these zones cannot be detected with sparse regional networks, and their definition requires densely distributed GPS arrays (~10–30 km spacing). In some cases, the deformation can be described by the motions of a small number of microplates. However, in contrast with deformation of oceanic plates, movements are often perturbed by high rates of straining in apparently isolated zones, potentially frustrating a simple microplate description of deformation kinematics.

Such kinematic behavior may be due to lateral variations in rheology and internal stresses that are intrinsic properties of the continental lithosphere. Differences in thermal history, rock type, and tectonism generate lateral variations in lithospheric strength. Tectonic and magmatic activity create lateral density gradients within the continental lithosphere that perturb local stresses and can themselves drive deformation. Deformation, once localized, will continue until local stress heterogeneities are relieved by density redistribution that accompanies deformation. Plate boundary and internal driving forces change with time, both abruptly and in small increments, leading to deactivation and migration of deforming zones.

REFERENCES

Argus, D. F., and Gordon, R. G., 1991, Current Sierra Nevada–North America motion from very long baseline interferometry: Implications for the kinematics of the western United States: Geology, v. 19, p. 1085–1088.

Atwater, T., and Stock, J., 1998, Pacific–North America plate tectonics of the Neogene southwestern United States: An update: International Geology Review, v. 40, p. 375–402.

Avouac, J.-P., and Tapponier, P., 1993, Kinematic model of active deformation in central Asia: Geophysical Research Letters, v. 20, p. 895–898.

Beavan, J., et al., 1999, Crustal deformation during 1994–1998 due to oblique continental collision in the central Southern Alps, New Zealand, and implications for seismic potential of the Alpine fault: Journal of Geophysical Research, v. 104, p. 25,233–25,255.

Bennett, R. A., Davis, J. L., and Wernicke, B. P., 1998, Continuous GPS measurements of deformation across the northern Basin and Range province: Geophysical Research Letters, v. 25, p. 563–566.

Bourne, S. J., et al., 1998, Crustal deformation of the Marlborough fault zone in the South Island of New Zealand: Journal of Geophysical Research, v. 103, p. 30147–30166.

Clarke, P. J., et al., 1998, Crustal strain in central Greece from repeated GPS measurements in the interval 1989–1997: Geophysical Journal International, v. 135, p. 195–214.

Cavinato, G. P., and De Celles, P., 1999, Extensional basins in the tectonically bimodal central Apennines fold-thrust belt, Italy: Response to corner flow above a subducting slab in retrograde motion: Geology, v. 27, p. 955–958.

Coblenz, D. D., Richardson, R. M., and Sandiford, M., 1994, On the gravitational potential of the Earth's lithosphere: Tectonics, v. 13, p. 929–945.

Cocard, M., et al., 1999, New constraints on the rapid crustal motion of the Aegean region: Recent results inferred from GPS measurements (1993–1998) across the West Hellenic Arc, Greece: Earth and Planetary Science Letters, v. 172, p. 39–47.

Demets, C., and Dixon, T. H., 1999, New kinematic models for Pacific–North America motions from 3 Ma to present: 1. Evidence for steady motion and biases in

the NUVEL-1A model: Geophysical Research Letters, v. 26, p. 1931–1934.

Demets, C., Gordon, R. G., Argus, D. F., and Stein, S., 1990, Current plate motions: Geophysical Journal International, v. 101, p. 425–478.

Demets, C., S. Gordon, S., and Royer, J.-Y., 2002, A new high-resolution model for India-Capricorn-Somalia plate motion since 20 Ma: Implications for chronology and magnitude of distributed seafloor deformation in the central Indian Basin: Geophysical Journal International, in press.

Dixon, T. H., Miller, M., Farina, F., Wang, H., and Johnson, D., 2000, Present-day motion of the Sierra Nevada block and some tectonic implications for the Basin and Range province, North American Cordillera: Tectonics, v. 19, p. 1–24.

England, P. C., and McKenzie, D. P., 1982, A thin viscous sheet model for continental deformation: Geophysical Journal of the Royal Astronomical Society, v. 70, p. 295–321.

England, P. C., Houseman, G. A., and Sonder, L., 1985, Length scales for continental deformation on convergent, divergent and strike-slip environments: Analytical and approximate solutions for a thin viscous sheet model: Journal of Geophysical Research, v. 90, p. 3351–3357.

Flesch, L. M., Holt, W. E., Haines, A. J., and Shen-Tu, B., 2000, Dynamics of the Pacific–North American plate boundary in the western United States: Science, v. 287, p. 834–836.

Forsyth, D., and Uyeda, S., 1975, On the relative importance of the driving forces of plate motion: Geophysical Journal of the Royal Astronomical Society, v. 43, p. 163–200.

Freymueller, J. T., Murray, M. H., Segall, P., and Castillo, D., 1999, Kinematics of the Pacific–North America plate boundary zone, northern California: Journal of Geophysical Research, v. 104, p. 7419–7441.

Gan, W., Svarc, J. L., Savage, J. C., and Prescott, W. H., 2000, Strain accumulation across the Eastern California shear zone at latitude 36° 30′ N: Journal of Geophysical Research, v. 105, p. 16,229–16,236.

Hammond, W. C., and Thatcher, W., 2001, Integrated kinematic analysis of GPS and fault slip data in the eastern California shear zone, Walker Lane, and Sierra Nevada: EOS (Transactions of the American Geophysical Union), v. 82, p. F280.

Jackson, J. A., 1994, Active tectonics of the Aegean region: Annual Reviews of Earth and Planetary Sciences, v. 22, p. 239–271.

Jones, C. H., Unruh, J. R., and Sonder, L. J., 1996, The role of gravitational potential energy in the active deformation of the southwestern United States: Nature, v. 381, p. 37–41.

Khazaradze, G., Qamar, T., and Dragert, H., 1999, Tectonic deformation in western Washington from continuous GPS measurements: Geophysical Research Letters, v. 23, p. 3153–3156.

Kohlstedt, D. L., Evans, B., and Mackwell, S. J., 1995, Rheology of the lithosphere: Constraints imposed by laboratory experiments: Journal of Geophysical Research, v. 100, p. 17,587–17,602, 1995.

Lachenbruch, A. H., and Morgan, P., 1990, Continental extension, magmatism and elevation: Formal relations and rules of thumb: Tectonophysics, v. 174, p. 39–62.

Le Pichon, X., 1982, Landlocked ocean basins and continental collision: The eastern Mediterranean as a case example, in Hsu, K., ed., Mountain building processes: San Diego, CA: Academic Press, p. 201–211.

Le Pichon, X., Chaqmot-Rooke, N., Lallemant, S., Noomen, R., and Veis, G., 1995, Geodetic determination of the kinematics of central Greece with respect to Europe: Journal of Geophysical Research, v. 100, p. 12,675–12,690.

Le Pichon, X., Mazzotti, S., Henry, P., and Hashimoto, M., 1998, Deformation of Japanese islands and seismic coupling: An interpretation based on GSI permanent GPS observations: Geophysical Journal International, v. 134, p. 501–514.

Lisowski, M., Savage, J. C., and Prescott, W. H., 1991, The velocity field along the San Andreas fault: Journal of Geophysical Research, v. 96, p. 8369–8389.

Matmon, A., Bierman, P., Larsen, J., Southworth, S., Pavich, M., and Caffee, M., 2003, Temporally and Spatially uniform rates of erosion in the southern Appalachian Mountains, Geology, v. 31, p. 155–158.

Mazzotti, S., Henry, P., and Le Pichon, X., 2001, Transient and permanent deformation of central Japan estimated by GPS: Earth and Planetary Science Letters, v. 184, p. 455–469.

Mazzotti, S., Le Pichon, X., Henry, P., and Miyazaki, S., 2000, Full interseismic locking of the Nankai and Japan–West Kurile subduction zones: An analysis of uniform elastic strain accumulation in Japan constrained by permanent GPS: Journal of Geophysical Research, v. 105, p. 13,159–13,177.

McCaffrey, R., et al., 2000, Rotation and plate locking at the southern Cascadia subduction zone: Geophysical Research Letters, v. 27, p. 3117–3120.

McKenzie, D. P., 1972, Active tectonics of the Mediterranean region: Geophysical Journal of the Royal Astronomical Society, v. 30, p. 109–185.

McKenzie, D. P., and Morgan, W. J., 1969, Evolution of triple junctions: Nature, v. 224, p. 125–133.

Minster, J. B., and Jordan, T. H., 1978, Present-day plate motions: Journal of Geophysical Research, v. 83, p. 813–821.

Mooney, W. D., Prodehl, C., and Pavlenkova, N., 2002, Seismic velocity structure of the continental lithosphere from controlled source data, in Lee, W. H. K., ed., International handbook of earthquake and engineering seismology, v. 81A, chapter 54, p. 887–910.

Mount, V. S. and Suppe, J., 1987, State of stress near the San Andreas fault: Implications for wrench tectonics: Geology, v. 15, p. 1143–1146.

Nishimura, T., et al., 2001a, Crustal deformation caused by magma migration in the northern Izu Islands, Japan: Geophysical Research Letters, v. 28, p. 3745–3748.

———, 2001b, Distribution of seismic coupling on the subducting plate boundary in northeastern Japan inferred from GPS observations: Tectonophysics, v. 323, p. 217–238.

Prescott, W. H., Savage, J. C., Svarc, J. L., and Manaker, D., 2001, Deformation across the Pacific–North America plate boundary near San Francisco, California: Journal of Geophysical Research, v. 106, p. 6673–6682.

Research Group for Active Faults in Japan, 1991, Active faults in Japan: Sheet maps and inventories , rev. ed.: Tokyo, Japan, University of Tokyo Press.

Richardson, R. M., and Reding, L. M., 1991 North American plate dynamics: Journal of Geophysical Research, v. 96, p. 12,201–12,223.

Richter, C., 1958, Elementary seismology: San Francisco, CA, W. H. Freeman, 768 p.

Royer, J.-Y., and Gordon, R. G., 1997, The motion and boundary between the Capricorn and Australian plates: Science, v. 277, p. 1268–1274.

Sagiya, T., 1999, Interplate coupling in the Tokai district, central Japan, deduced from continuous GPS data: Geophysical Research Letters, v. 23, p. 2315–2318.

Sagiya, T., S. Miyazaki, S., and Tada, T., 2000, Continuous GPS array and present-day crustal deformation in Japan: PAGEOPH (Pure and Applied Geophysics), v. 157, p. 2302–2322.

Sagiya, T., Nishimura, T., Iio, Y., and Tada, T., 2002, Crustal deformation around the northern Itoigawa-Shizuoka tectonic line: Earth, Planets, and Space, v. 54, p. 1059–1063.

Sagiya, T., and Thatcher, W. , 1999, Coseismic slip resolution along a plate boundary megathrust: The Nankai Trough, southwest Japan: Journal of Geophysical Research, v. 104, p. 1111–1129.

Savage, J. C., and Burford, R. O., 1973, Geodetic determination of relative plate motion in central California: Journal of Geophysical Research, v. 78, p. 832–845.

Savage, J. C., Svarc, J. L., and Prescott, W. H., 1999, Geodetic estimates of fault slip rates in the San Francisco Bay area: Journal of Geophysical Research, v. 104, p. 4995–5002.

Savage, J. C., Svarc, J. L., Prescott, W. H., and Murray, M. H., 2000, Deformation across the forearc of the Cascadia subduction zone at Cape Blanco, Oregon: Journal of Geophysical Research, v. 105, p. 3095–3102.

Sibson, R. H., 1985, A note on fault reactivation: Journal of Structural Geology, v. 7, p. 751–754.

Smith, R. B., and Arabaez, W. J., 1991, Seismicity of the Intermountain Seismic Belt: Geological Society of America, SMV V-1, Decade Map Volume 1, p. 185–228.

Sonder, L. J., and England, P. C., 1986, Vertical averages of rheology of the continental lithosphere: Earth and Planetary Science Letters, v. 77, p. 81–90.

Svarc, J. L., Savage, J. C., Prescott, W. H., and Ramelli, A. R., 2002, Strain accumulation and rotation in western Nevada: Journal of Geophysical Research, 2001JB000579.

Tabei, T. et al., 2002, Subsurface structure and faulting of the Median Tectonic Line, southwest Japan inferred from GPS velocity field: Earth, Planets, Space, v. 54, 1065–1070.

Tanioka, Y., Satake, K., and Ruff, L., 1995, Total analysis of the 1993 Hokkaido Nansei-oki earthquake using seismic wave, tsunami, and geodetic data: Geophysical Research Letters, v. 22, p. 9–12.

Thatcher, W., 1975, Strain accumulation on the northern San Andreas fault zone since 1906: Journal of Geophysical Research, v. 80, p. 4873–4880.

———, 1979a, Systematic inversion of geodetic data in central California: Journal of Geophysical Research, v. 84, p. 2283–2295.

———, 1979b, Horizontal crustal deformation from historic geodetic data in southern California: Journal of Geophysical Research, v. 84, p. 2351–2370.

———, 1990, Present-day crustal movements and mechanics of cyclic deformation, *in* Wallace, R. E., ed., The San Andreas Fault system, California: U. S. Geological Survey Professional Paper 1515, p. 189–205.

———, 1995, Continuum versus microplate models of active continental deformation: Journal of Geophysical Research, v. 100, p. 3885–3894.

Thatcher, W., Foulger, G. R., Julian, B. R., Svarc, J., Quilty, E., and Bawden, G. W., 1999, Present-day deformation across the Basin and Range Province, western United States: Science, v. 283, p. 1714–1718.

Valensise, G., and Pantosti, D., 2001, Database of potential sources for earthquakes larger than M 5.5 in Italy: Annali di Geophysica, v. 44, p. 797–964.

Walcott, R. I., 1978, Present tectonics and Late Cenozoic evolution of New Zealand: Geophysical Journal of the Royal Astronomical Society, v. 52, p. 137–164.

———, 1998, Modes of oblique compression: Late Cenozoic tectonics of the South Island of New Zealand: Review of Geophysics, v. 36, p. 1–26.

Wald, D. J., and Sommerville, P. G., 1995, Variable-slip rupture model of the Great 1923 Kanto, Japan Earthquake: Geodetic and body-waveform analysis: Bulletin of the Seismological Society of America, v. 85, p. 159–177.

Wells, R. E., Weaver, C. S., and Blakely, R. J., 1998, Forearc migration in Cascadia and its neotectonic significance: Geology, v. 26, p. 759–762.

Wernicke, B., and Snow, J. K., 1998, Cenozoic tectonism in the central Basin and Range: Motion of the Sierran–Great Valley block: International Geology Review, v. 40, p. 403–410.

Zoback, M. D. et al., 1987, New evidence on the state of stress of the San Andreas fault system, Science, v. 238, p. 1105–1111.

Zoback, M. D., and Townend, J., 2001, Implications of hydrostatic pore pressures and high crustal strength for the deformation of intraplate lithosphere: Tectonophysics, v. 336, p. 19–30.

Zoback, M. L., Anderson, R. E., and Thompson, G. A., 1983, Cenozoic evolution of the state of stress and style of tectonism of the Basin and Range province of the western United States: Philosophical Transactions of the Royal Society of London A, v. 300, p. 407–434.

Zoback, M. L., et al., 1989, Global patterns of tectonic stress, Nature, v. 341, p. 291–298.